Articles

Combining Theory and Experiment in Determining the Surface Chemistry of Nanocrystals

A. S. Barnard* and A. I. Kirkland†

Department of Materials, University of Oxford, Oxford, OX1 3PH, U.K.

Received January 21, 2008. Revised Manuscript Received July 8, 2008

The development of future generation catalysts and fuel cells based on oxide nanostructures is dependent upon our ability to control the size, shape, and surface chemistry of individual particles. It is currently not possible to characterize the surface of substantial numbers of oxide nanocrystals within large scale samples using exclusively experimental methods. In this paper, we outline a combined methodology for partnering advanced imaging techniques, to provide local experimental structural information, with multiscale computer modeling, to identify the terminal (surface) atomic layer, and apply this technique to the case of CeO_2 nanoparticles.

1. Introduction

The field of nanocatalysis has undergone explosive growth during the past decade, driven by the discovery that, due to their high surface area, oxide nanoparticles are more effective catalysts than their bulk counterparts. In particular, ceria (CeO_2) has attracted considerable interest due to its unique properties and applications in various aspects of nanocatalysis[1−4] and solid fuel cells.[5−7] Given the impending energy crisis and the current global dependence on fossil fuels for the automotive industry, possibly the most important (and immediate) application of ceria nanoparticles is as an efficient "oxygen buffer" in an automotive three-way catalyst (TWC).

These buffers are essential in stabilizing the air-to-fuel ratio necessary to achieve simultaneous conversion of NO, CO, and hydrocarbons during both the fuel-lean and fuel-rich stages of the combustion cycles.[8] Bulk ceria is known to be an excellent oxygen buffer,[9] and (high surface area) nanoparticles have been shown to achieve the desired redox efficiency.[10] However, significant technological problems arise as the particles size decreases, as ceria nanoparticles tend to aggregate (decreasing the effective surface area) with consequent degradation in catalytic performance.[10] This aggregation behavior is driven by the compatibility of the shape of individual nanoparticles (characterized by the relative fractions of different crystallographic facets[11] and their surface terminations) and can be substantially reduced by control of the shape of individual nanoparticles during synthesis.

Ceria nanoparticles may be prepared via thermal hydrolysis,[12] coprecipitation,[13,14] combustion,[15,16] microemulsion,[17−19] thermal decomposition,[20] and other techniques.[21−24] Each of these methods provides opportunities to tailor their shape through control of specific synthetic parameters such as temperature and the composition of precursors which influence the surface chemistry and surface structure. Unfortunately, the underlying relationships between these experi-

* Corresponding author. E-mail: amanda.barnard@materials.ox.ac.uk.
† angus.kirkland@materials.ox.ac.uk.

(1) Parthasarathi, B.; Aruna, S. T.; Patil, K. C.; Hegde, M. S. *J. Catal.* **1999**, *186*, 36.
(2) Fally, F.; Perrichon, V.; Vidal, H.; Kaspar, J. *Catal. Today* **2000**, *59*, 373.
(3) Florence, E.; Florence, G.; Jacques, B. *J. Catal.* **2002**, *206*, 363.
(4) Solinas, V.; Rombi, E.; Ferino, I.; Cutrufello, M. G. *J. Mol. Catal. A* **2003**, *204*, 629.
(5) Bellon, O.; Sammes, N. M.; Staniforth, J. *J. Power Sources* **1998**, *75*, 116.
(6) Natsuko, S.; Takuya, H.; Tomoyuki, K.; Katsuhiko, Y. *Solid State Ionics* **2001**, *143*, 151.
(7) Lu, C.; Worrell, W. L.; Wang, C.; Park, S. *Solid State Ionics* **2002**, *152*, 393.
(8) Yao, H. C.; Yu, Y. F. *J. Catal.* **1984**, *86*, 254.
(9) Taylor, K. C. *Catal. Rev. Sci. Eng.* **1993**, *35*, 3457.
(10) (a) Fornasiero, P.; Balducci, G.; Di Monte, R.; Kaspar, J.; Sergo, V.; Gubitosa, G.; Ferrero, A.; Graziani, M. *J. Catal.* **1996**, *164*, 173. (b) El Fallah, J.; Boujana, S.; Dexpert, H.; Kiennemann, A.; Majerus, J.; Touret, O.; Villain, F.; Le Normand, F. *J. Phys. Chem.* **1994**, *98*, 5522.
(11) Wang, Z. L.; Feng, X. *J. Phys. Chem. B* **2003**, *107*, 13565.
(12) (a) Hirano, M.; Kato, E. J. *Mater. Sci. Lett* **1996**, *15*, 1249. (b) Hirano, M.; Kato, E. *J. Am. Ceram. Soc.* **1996**, *79*, 777. (c) Hirano, M.; Inagaki, M. *J. Mater. Chem.* **2000**, *10*, 473.
(13) Kirk, T. J.; Winnick, J. *J. Electrochem. Soc.* **1993**, *140*, 3494.
(14) Muccillo, E.; Rocha, R.; Tadokoro, S.; Rey, J.; Muccillo, R. *J. Electroceram.* **2004**, *13*, 609.
(15) Sekar, M. M. A.; Manoharan, S. S.; Patil, K. C. *J. Mater. Sci. Lett.* **1990**, *9*, 1205.
(16) Purohit, R. D.; Sharma, B. P.; Pillai, K. T.; Tyagi, A. K. *Mater. Res. Bull.* **2001**, *36*, 2711.
(17) He, Y. J.; Yang, B.; Cheng, G. X. *Mater. Lett.* **2003**, *57*, 1880.
(18) Lee, J.-S.; Lee, J.-S.; Choi, S.-C. *Mater. Lett.* **2005**, *59*, 395.
(19) Kuiry, S. C.; Seal, S.; Vanfleet, R. *J. Nanoparticle Res.* **2002**, *4*, 433.
(20) Kamruddin, M.; Ajikumar, P. K.; Nithya, R.; Tyagi, A. K.; Raj, B. *Scripta Mater.* **2004**, *50*, 417.
(21) Hakuta, Y.; Onai, S.; Terayama, H.; Adschiri, T.; Arai, K. *J. Mater. Sci. Lett.* **1998**, *17*, 1211.
(22) Liang, C.; Qiu, J.; Li, Z.; Li, C. *Nanotechnology* **2004**, *15*, 843.
(23) Chavan, S. V.; Tyagi, A. K. *Ceram. Int.* **2005**, *31*, 731.
(24) Yang, H.; Huang, C.; Tang, A.; Zhang, X.; Yang, W. *Mater. Res. Bull.* **2005**, *40*, 1690.

10.1021/cm8001892 CCC: $40.75
Published on Web 08/14/2008

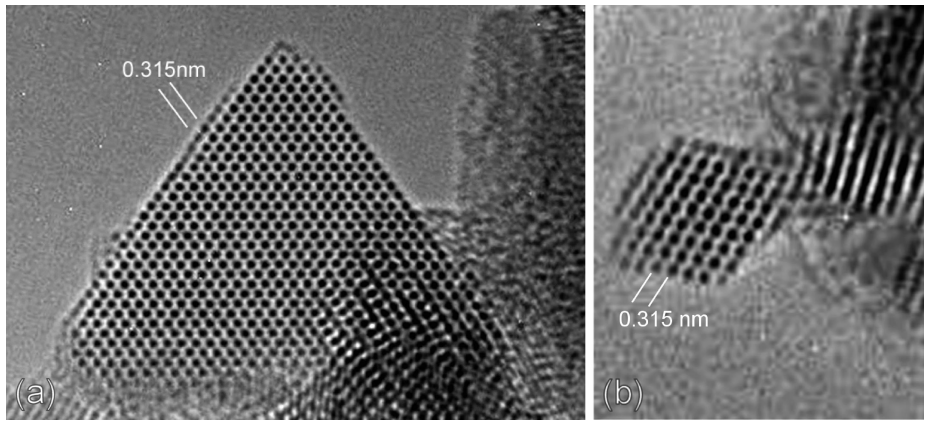

Figure 1. (a) HRTEM image of a typical ⟨110⟩ oriented CeO_2 particle with extended {111} facets and a small (4 atomic column width) apical {100} facet and (b) example of the smallest particles with apical {100} facets best described as low index surfaces formed from stepped {111} surfaces, all recorded at close to the Scherzer defocus condition at primary magnifications of between 300 000 and 500 000×.

mental parameters and the resulting nanoparticle shape are still poorly understood. Hence, improvements in the performance of ceria-based and other nanocatalysts will not be realized until a fundamental investigation as to how their shape is governed by the surface structure and surface chemistry is undertaken, so as to guide future synthesis efforts. In this regard, experimental characterization using electron microscopy is necessarily highly selective within a bulk sample and does not immediately provide predictive capability with respect to size and morphology. However using experimental data as a calibration for accurate theoretical models enables the effects of size and morphological changes on the surface structure to be predicted for a wide range of external conditions.

2. Experimental Details

Using advanced high resolution transmission electron microscopy (HRTEM), the structure and chemistry of a range of ceria nanocrystals has been investigated with the intention of characterizing the overall particle shape and surface structure. Specimens for TEM were prepared by dispersion of the as-synthesized CeO_2 powder[25] in propanol followed by sonication and a drop of the resultant suspension was subsequently allowed to dry on a TEM grid coated with a "holey" amorphous carbon support film. The nanoparticulate powders of CeO_2 were synthesized using combustion chemical vapor condensation, as described in detail elsewhere.[25] For the studies reported here, only CeO_2 particles synthesized by this method were examined although, as noted earlier, preparation conditions (and in particular the presence of precursor counterions) can have a significant effect on the developed particle morphology. Suitable oriented (generally ⟨110⟩) particles were examined in a 400 kV TEM (JEOL 4000EX) with an interpretable point resolution of 0.17 nm. Experimental images were recorded at close to the Scherzer defocus condition[37] at primary magnifications of between 300 000 and 500 000×. Initial screening of particles at low magnification gave a mean particle size of 4.6 ± 0.8 nm based on measurement of 63 particles with a clearly identifiable morphology in projection. We also note that within the as-synthesized sample there were also larger aggregates of particles present which were not analyzed.

Figure 1a shows a typical ⟨110⟩ oriented CeO_2 particle with extended {111} facets and a small (4 atomic column width) apical {100} facet. In Figure 1a, individual black spots correspond to unresolved O—Ce—O atom groups projected along a ⟨110⟩ direction, and at this resolution, is not possible to assign the surface termination as O or Ce. We note however that there is evidence for incomplete surface layers along the {111} facets of the crystal and for disorder on the apical {100} plane. However, during the course of our studies we have not observed any radiation induced changes or instabilities in the crystal and hence these local defects are assumed to be present in the as-synthesized material. We have imaged many similar crystals and in all cases the preferred morphology was one with extended {111} facets and small apical {100} facets. For the smallest particles imaged the apical {100} facets are best described as low index surfaces formed from stepped {111} surface, as shown in Figure 1b. On the basis of measurement of 16 HRTEM images, the ratio of {111}:{100} for 4−6 nm particles gives a mean ∼97 ± 1% {111} surface area.

These results demonstrate that although the terminal atomic layer cannot always be definitely identified, the shape of the nanocrystals (characterized in terms of the {100}/{111} ratio) can be relatively unambiguously determined. Fortunately, examining the relationship between surface structure and shape of nanocrystals is relatively straightforward using computer modeling. Since the nanocrystals are enclosed by {100} and {111} facets, which may be either oxidized or reduced, there are four possible combinations that could represent the surface structure of our specimens. Therefore, by modeling the shape and thermodynamic stability of nanocrystals with oxidized/reduced {100}/{111} facets and comparing the predicted shape with those observed, it is possible to indirectly determine which species occupy the terminal atomic (surface) layer. The combination of experimental shape determination and modeling provides the complete set of information required to comprehensively characterize oxide nanocrystals.

3. Theoretical Details

The computer modeling was carried out using a shape-dependent thermodynamic model based on a geometric summation of the Gibbs free energy[29] which has previously been successfully used to examine the shape of oxides.[30−32] The version of the model used here is applicable specifically to isolated, defect-free structures in the range ∼3−100 nm.[29] In this version, the total free energy G is described in terms

(25) Maric, R.; Oljaca, M.; Vukasinovic, B.; Hunt, A. T. *Mater. Manufac. Proc.* **2004**, *19*, 1143.

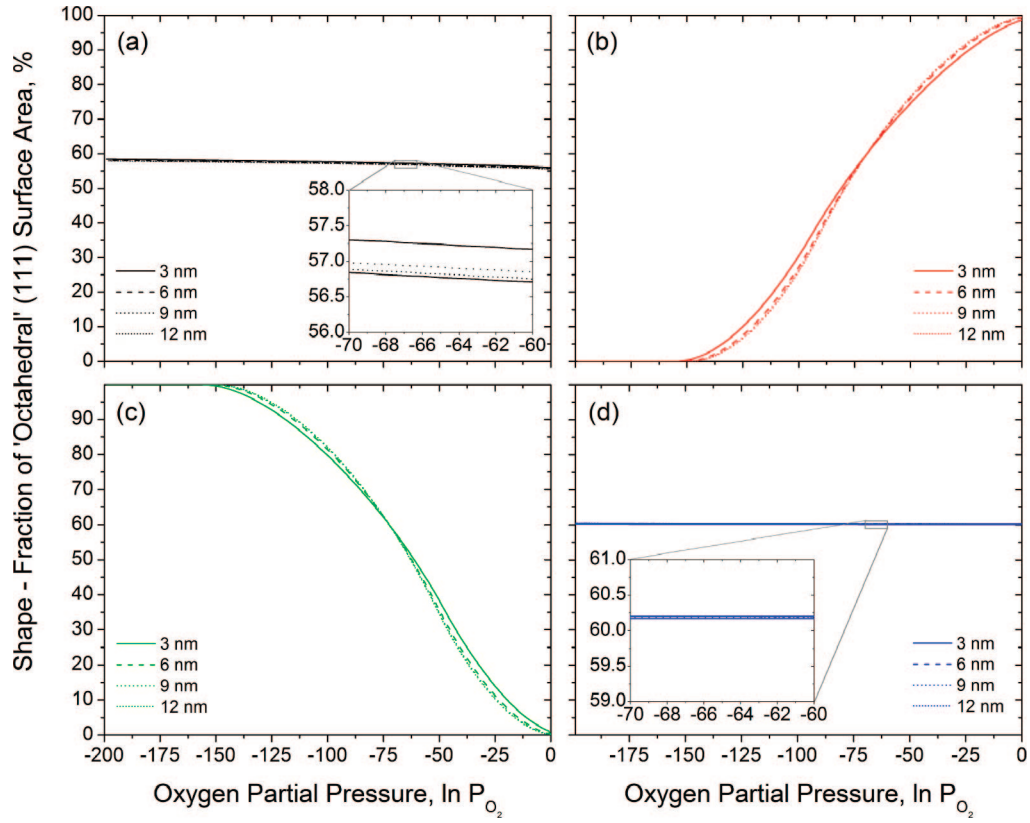

Figure 2. Predicted shape (in terms of the percent (111) surface area) as a function of oxygen partial pressure (P_{O_2}), with (a) oxidized {111} and {100} facets, (b) oxidized {111} and reduced {100} facets, (c) oxidized {100} and reduced {111} facets, and (d) reduced {100} and {111} facets.

of the specific surface free energies γ_i, for facets i, weighted by the factors f_i (such that $\Sigma_i f_i = 1$):

$$G = \Delta G_f^\circ + \frac{M}{\rho}\left(1 - \frac{2\sum_i f_i \sigma_i}{B_0 R} + \frac{P_{ex}}{B_0}\right)\left[q\sum_i f_i \gamma_\iota\right] \qquad (1)$$

where M is the molar mass, ρ is the density, and the volume dilation induced by the isotropic surface stresses σ_i and external pressure P_{ex} is included using the Laplace−Young formalism.[29] In all cases, atmospheric external pressure was assumed.

The parameters required for the Gibbs free energy summation are the specific surface free energies and the isotropic surface stresses. We have used the set of ab initio surface energies for the reconstructed {100} and {111} surfaces of ceria calculated by Jiang et al., using density functional theory (DFT) evaluated within the generalized gradient approximation using the Perdew−Burke−Ernzerhof (PBE) exchange-correlation functional and projected augmented wave (PAW) potentials for Ce and O atoms.[33] In order for the surface energies to be useful in experimental situations, these authors have expressed the surface energy in terms of the partial pressure of oxygen P_{O_2}, giving the nonstoichiometric surface formation energy, as follows:

$$\gamma_i(P_{O_2}) = \frac{1}{2A_i}\left[E_{total,i} - N_{Ce}\mu^0_{CeO_2,bulk} + (N_{Ce} - N_{O_2})\times \left(\mu^0_{CeO_2,bulk} - \mu^0_{Ce,bulk} - \Delta H^0_{f,bulk}\right) + (N_{Ce} - N_{O_2})kT \ln P_{O_2}\right] \qquad (2)$$

where,

$$\frac{\Delta H^0_{f,bulk}}{kT} < \ln P_{O_2} < 0 \qquad (3)$$

All chemical potentials ($\mu^0_{CeO_2,bulk}$ and $\mu^0_{Ce,bulk}$) and energies ($E_{total,i}$ and $\Delta H^0_{f,bulk}$) were approximated by calculations at 0 K, and the value of $\Delta H^0_{f,bulk} = -10.4$ eV was shown to be in excellent agreement with experimental measurements under ambient conditions. Therefore, using Jiang's results for $\gamma_i(P_{O_2})$ (together with eq 1), we are able to predict the shape of nonstoichiometric ceria nanostructures as a function of P_{O_2}. In each case, the effects of surface stress on the total free energy have been tested by comparing results calculated with $\sigma_i = 0$ and $\sigma_i = \gamma_i$, $\forall$ i. These tests indicated that, at the sizes discussed here, the affect of surface stress is small but may still be significant, so we have used the approximation $\sigma_i = \gamma_i$ as first approximation. It is also important to point out that the quantities were here were those corresponding to 300 K.[33] This implies that the specific results presented here are more related to low-temperature quasi-

(26) Hutchison, J. L.; Titchmarsh, J. M.; Cockayne, D. J. H. C.; Doole, R. C.; Hetherington, C. J. D. H.; Kirkland, A. I.; Sawada, H. *Ultramicroscopy* **2005**, *103*, 7.
(27) Chang, L. Y.; Kirkland, A. I.; Titchmarsh, J. M. *Ultramicroscopy* **2005**, *106*, 301.
(28) Jia, C. L.; Lentzen, M.; Urban, K. *Science* **2003**, *299*, 870.
(29) (a) Barnard, A. S.; Zapol, P. *J. Chem. Phys.* **2004**, *121*, 4276. (b) Barnard, A. S. *J. Phys. Chem. B* **2006**, *110*, 24498.
(30) (a) Barnard, A. S.; Zapol, P. *Phys. Rev. B* **2004**, *70*, 23540. (b) Barnard, A. S.; Zapol, P.; Curtiss, L. A. *J. Chem. Theo. Comp.* **2005**, *1*, 107.
(31) Barnard, A. S.; Curtiss, L. A. *Nano Lett.* **2005**, *5*, 1261.
(32) Barnard, A. S.; Yeredla, R. R.; Xu, H. *Nanotechnology* **2006**, *17*, 3039.
(33) Jiang, Y.; Adams, J. B.; van Schilfgaarde, M. *J. Chem. Phys.* **2005**, *123*, 064701.

equilibrium conditions and not to cases where ceria nanocrystals are grown at high temperature.

4. Discussion of Results

Using the expression given in eq 1 and the set of values for a, B_0, γ_i, and σ_i given in ref 33, the predicted equilibrium shape of a ceria nanocrystals over a range of diameters is shown in Figure 2. Each of the four possible surface combinations is represented, with oxidized {111} and {100} facets shown in Figure 2a, oxidized {111} and reduced {100} facets shown in Figure 2b, oxidized {100} and reduced {111} facets shown in Figure 2c, and reduced {100} and {111} facets shown in Figure 2d. In each case the shape is described by the fraction of {111} surface area. Since the samples were grown using hydrothermal synthesis techniques, we have restricted the model results to supersaturations close to equilibrium, where ln P_{O_2} is close to zero.

From this collection of data, a number of interesting trends can be discerned. First, when the degree of oxidation/reduction is isotropic over the entire surface of the particle (being either all O-terminated or all Ce-terminated), the shape of the particle is largely independent of both the oxygen partial pressure and the particle size. We can also see from Figure 2a and d that the predicted shape is intermediate between a truncated octahedron (with ~76% (111) surface area) and a regular cuboctahedron (with ~36% (111) surface area). For cases of anisotropic surface oxidation, the shape is highly dependent on the oxygen partial pressure, but still changes very little as a function of size. When the {100} facets are oxidized and the {111} facets are reduced the shape changes from an octahedron to a cube as ln P_{O_2} decreases from 0 to −150, whereas when the {111} facets are oxidized and the {100} facets are reduced the shape changes from a cube to an octahedron over the same range.

Clearly anisotropic surface oxidation is required to maintain consistency with our experimental observations. Furthermore, given that the our nanoparticles were not synthesized under reducing conditions (and the electron beam is the only reducing medium present during characterization), we can conclude that our ceria nanoparticles are most likely to be O-terminated on the majority (111) surfaces, but Ce-terminated on the minority apical (100) facets. We may even infer the oxygen partial pressure present during synthesis to be approximately ln $P_{O_2} = -9$.

5. Conclusion

Therefore, we demonstrated here by using accurate experimental characterization of the shape of ceria nanocrystals as input into a shape-dependent thermodynamic model, that it is possible to determine the detailed surface chemistry of ceria at the nanoscale. This simple (but general) methodology can be easily applied to any oxide nanostructure and may prove invaluable in cases where local high resolution information is not available and direct assignment of the surface termination is not possible. Future work on this type of combined methodology will be focused on examining the affect of surfactants on the shape of ceria nanocrystals, since it is also impossible to image the position, type, and degree of coverage of molecular adsorbates directly using electron microscopy.

Acknowledgment. This work has been supported by the Glasstone Benefaction at the University of Oxford. We also acknowledge financial support from EPSRC, and we would also like to acknowledge the support of John Hutchison and Peter Dobson.

CM8001892

(34) Nolan, M.; Grigoleit, S.; Sayle, D. C.; Parker, S. C.; Watson, G. W. *Surf. Sci.* **2005**, *576*, 217.
(35) Nolan, M.; Parker, S. C.; Watson, G. W. *Surf. Sci.* **2005**, *595*, 223.
(36) Sayle, T. X. T.; Parker, S. C.; Sayle, D. C. *Chem. Commun.* **2004**, 2438.
(37) Scherzer, O. *J. Appl. Phys.* **1949**, *20*, 20.